

Static computational micromagnetism of demagnetization processes in nanoscaled permanent magnets

R. Fischer and H. Kronmüller

Max-Planck-Institut für Metallforschung, Institut für Physik, Postfach 80 06 65, D-70569 Stuttgart, Germany

(Received 29 December 1995)

Micromagnetic calculations using the finite-element method provide a quantitative understanding of demagnetization processes in nanocrystalline ferromagnetic materials. In these materials demagnetization processes are mainly determined by short-range exchange and long-range dipolar interactions, which sensitively depend on microstructural properties. To reveal the relations between intergrain interactions, microstructure and magnetic properties like remanence and coercive field, we calculated the demagnetization curves for different three-dimensional grain structures as a function of the mean grain diameter: Starting from a single sphere, we successively constructed regular grain structures with increasing number of grains. The most complex grain arrangement consists of an ensemble of 35 isotropically distributed grains with disturbed surfaces. [S0163-1829(96)04633-4]

I. INTRODUCTION

Mechanically alloyed or melt-spun permanent magnets are based on ensembles of small polyhedral grains with isotropic distribution of easy axes.¹⁻¹³ In addition to the magnetic properties of each individual particle, intergrain interactions play a dominant role during demagnetization processes.¹⁴⁻¹⁹ These intergrain interactions are sensitively influenced by intergranular phases depending on the respective preparation method.²⁰⁻²⁴ A systematic improvement of permanent magnets is only possible by a deeper understanding of the relations between intergrain interactions, microstructural features, and magnetic properties. In this point of view, numerical calculations may provide us with important information on the role of these different relationships.

This paper gives a short review about fundamental demagnetization processes in nanoscaled Nd₂Fe₁₄B magnets and involves the effect of disturbed grain surfaces. In the framework of micromagnetism, we numerically investigated the following three-dimensional grain arrangements: a single sphere and cube with different alignments to the applied field, 35 directly contacted grains with a Gaussian distribution of the orientation of easy axes, 35 directly contacted grains with an isotropic distribution of the orientation of easy axes, and 35 isotropically distributed grains with different grain boundary types. For all grain structures the mean grain diameter was varied between 10 and 120 nm at room temperature.

II. THEORETICAL BACKGROUND

A. Characteristic properties of permanent magnets

The hysteresis loop of permanent magnets can be characterized by the remanence J_r , the coercive field H_c , and the maximum energy product $(BH)_{\max}$. The following sections briefly describe these quantities.

1. Remanence

According to the Stoner-Wohlfarth model²⁵ the saturation polarization J_{sat} of an ensemble of uniformly magnetized iso-

tropically distributed single-domain particles without any intergrain interactions, is given by^{4,26}

$$J_r = J_{\text{sat}} \frac{\int_0^{2\pi} \int_0^{\pi/2} \cos \vartheta_0 \sin \vartheta_0 d\vartheta_0 d\varphi_0}{\int_0^{2\pi} \int_0^{\pi/2} \sin \vartheta_0 d\vartheta_0 d\varphi_0} = 0.5 J_{\text{sat}}, \quad (1)$$

where J_{sat} denotes the saturation magnetization and ϑ_0 and φ_0 are the polar and azimuthal angles of the easy directions with respect to the applied field. So we expect for an ensemble of isotropically distributed isolated grains a remanence J_r half the saturation polarization J_{sat} .

2. Coercive field

In the scope of micromagnetism a simple approach to magnetization reversal processes is due to Brown, Stoner, and Wohlfarth.²⁵ Under the assumption of uniform demagnetization processes, the coercive field of an ideal-oriented spherical particle is given by the ideal nucleation field²⁷

$$H_N^{(0)} = \frac{2K_1}{J_s}, \quad (2)$$

where K_1 denotes the first anisotropy constant and J_s the spontaneous magnetic polarization. Actually, the coercive field of an ensemble of polyhedral grains is reduced to $0.3-0.5H_N^{(0)}$.²⁸ This can be attributed to microstructural features like misoriented grains, intergrain interactions, intergranular phases, and deteriorated grain surfaces.

3. Maximum energy product

The energy product $(BH)_{\max}$ is defined by the maximum scalar product of the magnetic flux density $B = \mu_0 H + J$ and the internal field $H = H_{\text{ext}} + H_d$ of the permanent magnet in the second quadrant of the hysteresis loop. The internal field H is the sum of the applied field $H_{\text{ext}} (< 0)$ and the macroscopic demagnetization field $H_d = -N(J/\mu_0)$. The demagnetization factor N can be numerically calculated and is of the order of 1/3 for cubic permanent magnets.²⁹ Since the maxi-

imum energy product is given by the maximum rectangle under the $B(H)$ loop, it is a useful measure of the performance of a particular permanent magnet. The maximum energy product increases with the remanence, if the coercive field is sufficiently high.^{30,31} Furthermore, the shape of the hysteresis loop should be as rectangular as possible. In this case $(BH)_{\max} = (1/4\mu_0)J_r^2$ holds.

B. Simulation model

The numerical simulation model to investigate magnetization processes in ferromagnetic is based on the continuum theory of micromagnetism. By means of the finite-element method, the minimization of the total magnetic Gibbs free energy^{28,32}

$$\Phi_t[\mathbf{J}_s(\vartheta(\mathbf{r}), \varphi(\mathbf{r}))] = \int d^3r \underbrace{\{A[(\nabla\vartheta(\mathbf{r}))^2 + (\nabla\varphi(\mathbf{r}))^2 \sin^2\vartheta(\mathbf{r})]\}}_{\text{exchange energy}} \quad (3)$$

$$+ \underbrace{K_1 \sin^2\alpha(\vartheta(\mathbf{r}), \varphi(\mathbf{r})) + K_2 \sin^4\alpha(\vartheta(\mathbf{r}), \varphi(\mathbf{r}))}_{\text{anisotropy energy}} \quad (4)$$

$$- \underbrace{\mathbf{J}_s(\vartheta(\mathbf{r}), \varphi(\mathbf{r}))\mathbf{H}_{\text{ext}}}_{\text{magnetostatic energy}} \quad (5)$$

$$- \underbrace{(1/2\mu_0)\mathbf{J}_s(\vartheta(\mathbf{r}), \varphi(\mathbf{r}))\mathbf{H}_s(\vartheta(\mathbf{r}), \varphi(\mathbf{r}))}_{\text{strayfield energy}}, \quad (6)$$

with respect to the polar coordinates $\vartheta(\mathbf{r})$ and $\varphi(\mathbf{r})$ of the spontaneous magnetic polarization \mathbf{J}_s yields a stable equilibrium states for the magnetization distribution of uniaxial magnetic materials. The only input to calculate the magnetization distribution are the grain structure (mean grain diameter $\langle D \rangle_{\text{grain}} \approx 10\text{--}120$ nm, diameter of intergranular layers $D_{\text{layer}} = 3$ nm, shape of polyhedral grains, easy axes distribution) and the material parameters of $\text{Nd}_2\text{Fe}_{14}\text{B}$ (spontaneous magnetic polarization $|\mathbf{J}_s| = J_s = 1.61$ T, exchange constant $A = 7.70 \times 10^{-12}$ J/m, first anisotropy constant $K_1 = 4.30 \times 10^6$ J/m³, and second anisotropy constant $K_2 = 0.65 \times 10^6$ J/m³) at $T = 300$ K.³³ The strayfield \mathbf{H}_s and the angle α between the spontaneous magnetic polarizations and the corresponding easy axis depend both on \mathbf{J}_s and therefore on $\vartheta(\mathbf{r})$ and $\varphi(\mathbf{r})$. A more detailed description of the used numerical method has been given in Ref. 34.

To calculate the demagnetization curve in the framework of static micromagnetism, we start the minimization of the total magnetic Gibbs free energy for a high saturation field and successively decrease the applied field. It is reasonable to use the preceding magnetization distribution as an initial guess for the iterative minimization process. For minimization, the so-called preconditioned, limited memory quasi-Newton conjugate gradient method³⁵ is proved to be most

successful. This method combines the advantages of the conjugate gradient method with the Newton method and uses curvature information. By adding a small random perturbation to the magnetization distribution, the coercivity can decrease between 0 and 10 %. Changes only exist at the irreversible part of the demagnetization curve and do not depend on the particular small perturbation.

In dynamic micromagnetism, the equation of motion for the spontaneous polarization in an effective field is usually solved to obtain both equilibrium and transient magnetization configurations.^{36–44} Frequently used are the Landau-Lifshitz or Landau-Lifshitz-Gilbert equation with physically different dissipative terms.⁴⁵ Several groups^{38,39} working on thin films emphasized the importance of the dynamical evolution of the magnetic moment especially as it switches. Depending on the particular microstructure and the ratio between the damping and anisotropy constant, the coercivity can be reduced between 0 and 30 %. It is important to note that by neglecting the gyroscopic motion of the magnetization vector the remanence always keeps constant and the coercivity surely does not increase. The quasistatistical results generally corresponds to dynamical calculations with high damping constant. Furthermore, the present micromagnetic algorithm does not take into account thermally activated

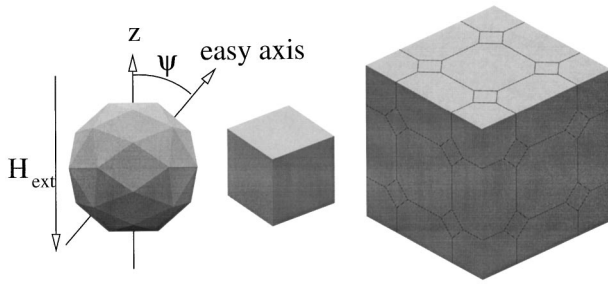


FIG. 1. Investigated grain structures consisting of $\text{Nd}_2\text{Fe}_{14}\text{B}$ grains (left: quasispherical grain, middle: cubic grain, right: ensemble of 35 regular grains). Ψ denotes the angle between the z axis and the easy axis.

processes.⁴⁶ If energy barriers vanish by thermal fluctuations of fine ferromagnetic particles, the coercivity can be additionally reduced.⁴⁷ So the coercivity represents at least a reliable upper bound by using the conjugate gradient method and neglecting thermal activation. But the incorporation of dynamically and thermally activated processes into the simulation program may be an interesting project for future.

Because of the simultaneous treatment of nonuniform magnetization distributions within each grain by using an adaptive mesh refinement and fully intergranular interaction, the static calculations without thermal activation reveal the relationship between details of the microstructure and magnetic properties like the remanence and the upper bound of the coercivity. That is exactly the aim of this paper. The computation time to obtain a demagnetization curve is of about 20–30 CPU h on a Cray-YMP for a complex three-dimensional grain structure. That means over 100 CPU h on a conventional alpha workstation.

III. FUNDAMENTAL DEMAGNETIZATION PROCESSES IN NANOSCALED PERMANENT MAGNETS

Demagnetization processes in ferromagnetic materials are mainly controlled by the magnetocrystalline anisotropy, strayfield effects and exchange interactions. In this section, we describe only the fundamental mechanisms determining the remanence and coercive field for nanoscaled grain structures shown in Fig. 1.

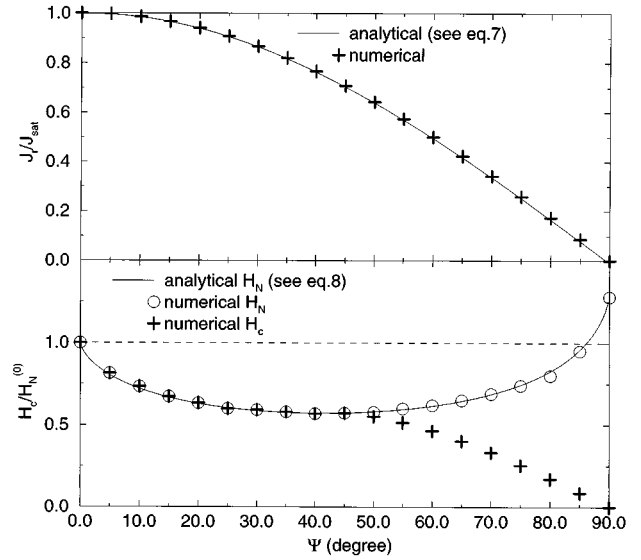


FIG. 2. Normalized remanence J_r/J_{sat} and coercive field $H_c/H_N^{(0)}$ as a function of the misorientation Ψ . J_{sat} denotes the saturation polarization and $H_N^{(0)}$ is the ideal nucleation field $2K_1/J_s$.

A. Single particles

1. Misoriented sphere

The quasispherical $\text{Nd}_2\text{Fe}_{14}\text{B}$ grain of Fig. 1 with a mean diameter of about 10 nm behaves like a Stoner-Wohlfarth particle. The strayfield distribution within spheres is uniform. If the angle Ψ between the easy axis of the magnetical uniaxial material and the applied field is zero, the remanence J_r equals the saturation polarization ($J_r = J_{\text{sat}} = J_s = 1.61$ T) and the coercive field is identical with the ideal nucleation field ($H_c = H_N^{(0)} = 2K_1/J_s \approx 6.3$ T). The magnetization reversal is spontaneous and uniform. Figure 2 shows the remanence and coercive field as a function of the misorientation Ψ between 0° and 90° . As expected, the remanence decreases according to

$$J_r = J_{\text{sat}} \cos \Psi \quad (7)$$

and is exactly zero at $\Psi = 90^\circ$. In the remanent state, all magnetic moments are perfectly aligned parallel to the direction of the easy axis. Between $0^\circ < \Psi < 45^\circ$, the coercive field is given by Ref. 48 to

$$H_c = H_N(\Psi) = H_N^{(0)} \frac{1}{[(\cos \Psi)^{2/3} + (\sin \Psi)^{2/3}]^{3/2}} \left[1 + \frac{2K_2}{K_1} \frac{(\tan \Psi)^{2/3}}{1 + (\tan \Psi)^{2/3}} \right]. \quad (8)$$

For values of Ψ greater than 45° the nucleation field $H_N(\Psi)$ starts to increase, whereas the coercive field still decreases (see Fig. 2). At $\Psi = 90^\circ$, the coercive field must be zero because all z components of the magnetic moments already vanish at $H_{\text{ext}} = 0$.

2. Cubic grain

The middle of Fig. 1 shows a cubic $\text{Nd}_2\text{Fe}_{14}\text{B}$ grain. The easy axis is assumed to be parallel to the z axis, which coincides with the applied field direction. The grain diameter $\langle D \rangle_{\text{grain}}$ is defined as the edge length of the cube. In contrast

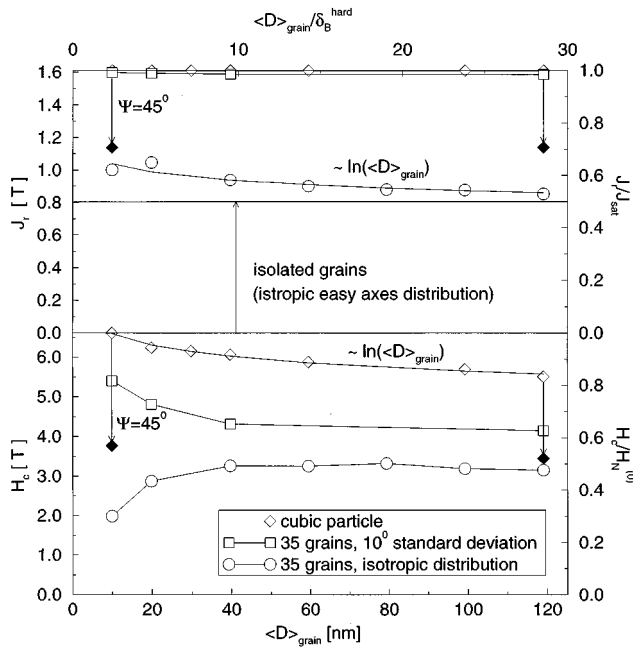


FIG. 3. Grain-size dependence of the remanence and of the coercive field for the cubic grain (diamonds) and 35 regular particles (squares and circles), which are presented in Fig. 1. The filled diamonds (at 10 and 120 nm) belong to the cube with an angle of 45° between the applied field and the direction of the easy axis.

to spheres, the strayfield within cubes is no longer uniform as shown previously by Schmidts and Kronmüller by presuming of quadratic cross sections.^{49,50} Also Schabes and Bertram⁵¹ and Uesaka, Nakatani, and Hayashi⁵² found non-uniform magnetization distributions for cubes by solving the dynamical problem. Figure 3 shows the results for the remanence and coercive field with increasing grain diameter (see diamonds). The remanence almost keeps constant, whereas the coercive field decreases logarithmic. The demagnetization process can be described as follows: Since the direction of the easy axis coincides with the direction of the applied field, the magnetic moments remain oriented in the z direction for decreasing external field. So we expect a remanence, which equals the saturation polarization ($J_r = J_{\text{sat}} = J_s = 1.61$ T). According to Fig. 4, the magnetization distribution for the remanent state ($H_{\text{ext}}=0$) actually shows deviations from a complete alignment parallel to the easy axis. Near sharp edges and corners, the magnetic moments are rotated into the local strayfield directions. Strayfield effects generally become more important with increasing particle size (compare both vector images of Fig. 4). But in nanoscaled dimensions, the remanence is not significantly reduced due to such local strayfields near edges and corners of the cubic particle (see also Fig. 3). This changes with increasing applied field in negative z direction. The inhomogeneous magnetization distributions near edges and corners cause an enhancement of the exchange and anisotropy energy. Therefore, the magnetization reversal takes place at smaller applied fields than for a uniform magnetization distribution. The reduction of the coercive field due to strayfield effects is negligible for small grains of about 10 nm and attains 16% of the ideal nucleation field for grains of about 120 nm.

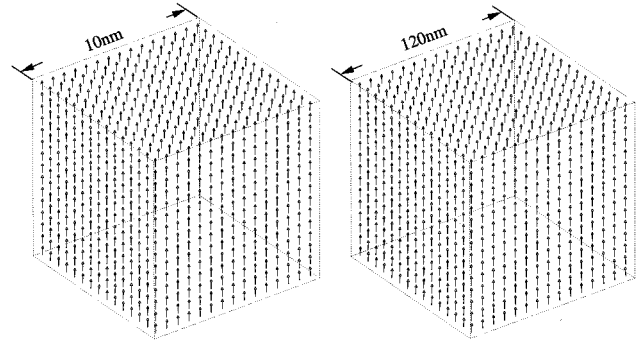


FIG. 4. Magnetization distributions for the cube at the remanent state ($H_{\text{ext}}=0$). The magnetic moments deviate from the z direction near sharp edges and corners. This effect is small in nanoscaled dimensions and only visible for large edge lengths of the cubic particle.

Figure 3 shows also the remanence and coercive field of the misoriented cube ($\Psi=45^\circ$) for two different grain sizes ($\langle D \rangle_{\text{grain}}=10$ nm, 120 nm). As described in Sec. III A 1, the misorientation strongly reduces the remanence as well as the coercive field. According to Fig. 3, demagnetization processes in nanoscaled dimensions are more influenced by the misorientation of the cube than by local strayfields.

B. Ensembles of grains

1. Gaussian distribution of easy axes

The next complex grain arrangement of Fig. 1 consists of 35 regular $\text{Nd}_2\text{Fe}_{14}\text{B}$ particles. The mean standard deviation of the Gaussian distribution of easy axes is of about 10° . All grains are in direct contact and their surfaces are assumed to be perfect without any inhomogeneity of the material parameters like exchange constant, magnetocrystalline anisotropy or spontaneous magnetic polarization. The grain diameter is defined by the diameter of a sphere with equal volume. The mean grain diameter of the grain structure is then the arithmetic average over all sphere diameters. To change the grain diameter, we just varied the edge length of the cubic magnet.

Figure 3 shows the remanence and coercive field as a function of the mean grain diameter (see squares). Similar to the cubic particle of Sec. III A 2, the remanence does not significantly deviate from the saturation polarization for all grain sizes between 10 and 120 nm. With decreasing external field, the magnetic moments turn into the directions of the easy axes within each grain. But this leads not to a remarkable decrease of the remanence, because of the small deviations of the easy axes with respect to the z direction (see magnetization distributions of Fig. 5).

According to Fig. 3, the coercive field decreases from $0.82H_N^{(0)}$ at $\langle D \rangle_{\text{grain}}=10$ nm to $0.63H_N^{(0)}$ at $\langle D \rangle_{\text{grain}}=120$ nm. In contrast to the cubic particle of Sec. III A 2, the decrease is not log-arithmically. With increasing applied field in negative z direction, the small misorientations of the grains become more important. As described in Sec. III A 1, the coercive field of each particle decreases with increasing misorientation. For a misorientation of 10° , the coercive field of a sphere is already reduced to $0.70H_N^{(0)}$. The decrease of the coercive field with increasing grain size may be attrib-

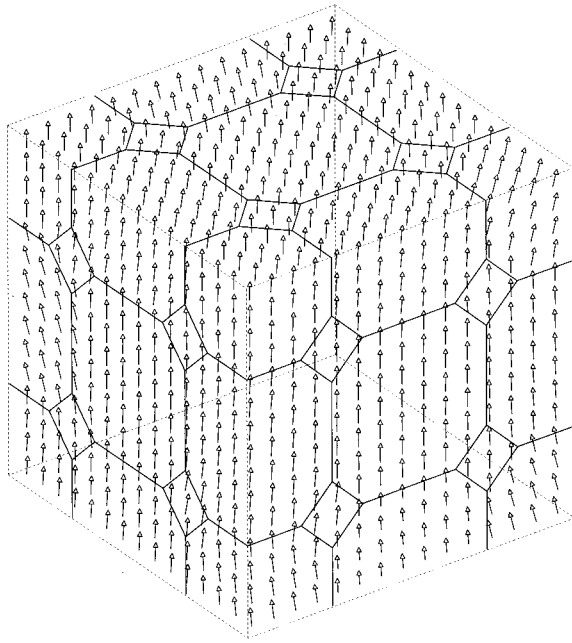


FIG. 5. Magnetization distribution for the ensemble with 35 grains and a Gaussian distribution of easy axes (10° standard deviation) at the remanent state ($H_{\text{ext}}=0$). The mean grain diameter is of about 120 nm. Most magnetic moments are nearly aligned parallel to the z direction.

uted to increasing local strayfields. In the case of small misorientations between neighboring grains, intergrain exchange interactions only play a minor role.

2. Isotropic distribution of easy axes

Now we investigate the 35 regular $\text{Nd}_2\text{Fe}_{14}\text{B}$ grains of Fig. 1 with an isotropic distribution of easy axes. In contrast to oriented magnets, exchange interactions play a dominant role during the demagnetization process. Especially for mean grain diameters smaller than 20 nm, the range of exchange interactions ($\delta_B \approx 4.2$ nm for $\text{Nd}_2\text{Fe}_{14}\text{B}$) is sufficiently large to reach significant volume parts of each grain. Exchange interactions generally suppress strong nonuniform magnetization distributions and so provide a smooth transition of the magnetization directions between adjacent misoriented grains.

Figure 3 shows the remanence and coercive field for the isotropic case as a function of the mean grain diameter (see circles). Compared to the grain structure of Sec. III B 1, both the remanence and coercive field are significantly reduced with respect to the saturation polarization and the ideal nucleation field. At the saturated state, all magnetic moments are parallel to the applied field in the z direction. With decreasing external field the magnetic moments rotate more and more into the directions of the easy axes, which are isotropically distributed. For the remanent state ($H_{\text{ext}}=0$), all magnetic moments within the grains are exactly aligned parallel to the corresponding directions of easy axes, if intergrain interactions do not exist. In this case Stoner and Wohlfarth calculated a remanence of $0.5J_{\text{sat}}$. But Fig. 3 shows a remanence of $0.63J_{\text{sat}}$ for $\langle D \rangle_{\text{grain}} \approx 10$ nm, which logarithmically decreases and reaches a value of about $0.53J_{\text{sat}}$ at

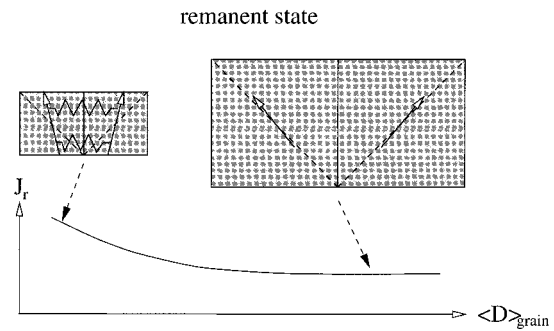


FIG. 6. Explanation of the relation between remanence and mean grain diameter for isotropic permanent magnets. The exchange interaction between neighbouring grains is responsible for the deviation of magnetic moments (arrows) from the directions of easy axes (dashed diagonals).

$\langle D \rangle_{\text{grain}} \approx 120$ nm. This remanence enhancement is a consequence of the competitive effects of magnetocrystalline anisotropy within each grain and the exchange interactions between neighboring grains. The relative strength of these two fundamental interactions mainly determine the magnetization distribution (and therefore the remanence) of nanoscaled isotropic permanent magnets. For small grains of about 10 nm, the range of exchange interactions is large enough to turn out the magnetic moments of the easy axes more in the z direction within a significant volume fraction between adjacent grains. According to the schematic Fig. 6, the resulting magnetic polarization in the z direction and hence the remanence increases. With increasing grain diameter the remanence enhancement decreases because the intergrain exchange interactions become less effective (see schematic, Figs. 6 and 3).

By applying an external field into the negative z direction, the magnetic moments turn more and more parallel to the easy axes, even at grain boundaries. For an isotropic distribution of easy axes always extremely misoriented grains exist near 90° with respect to the z direction. Since exchange interactions suppress strong inhomogeneous magnetization distributions, the magnetic moments of the surrounded grains rotate near the grain junctions over their easy axes directions more into the negative z direction (see schematic, Fig. 7).

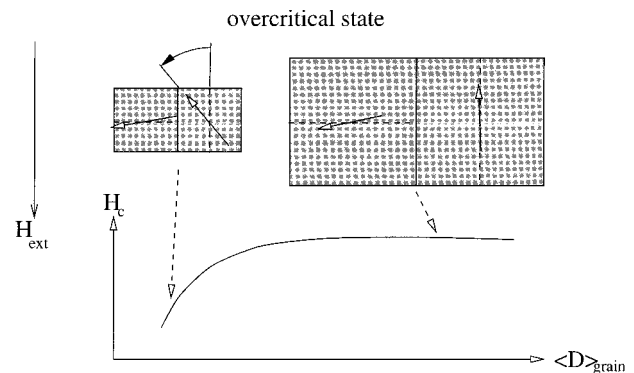


FIG. 7. Explanation of the relation between coercive field and mean grain diameter for isotropic permanent magnets. The dashed lines indicate the direction of the easy axes. The schematic picture describes the situation a little before magnetization reversal (overcritical state).

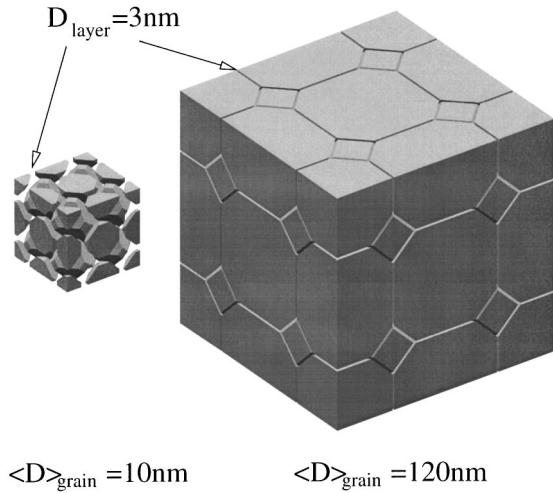


FIG. 8. Grain structure with intergranular layers. The volume fraction of intergranular phases decreases with the grain diameter (see also Fig. 9).

With further increasing external field, magnetization reversal takes place at first at grains surrounding the extremely mis-oriented one.¹⁹ So extremely misoriented grains cause magnetization reversal of exchange-coupled environments and reduce the coercive field. This effect becomes less effective if the range of exchange interactions becomes small with respect to the grain diameter: the coercive field increases with the grain size (see schematic, Figs. 7 and 3).

IV. EFFECT OF INTERGRANULAR PHASES ON DEMAGNETIZATION PROCESSES IN NANOSCALED ISOTROPIC MAGNETS

According to experimental investigations of grain structures of nanocrystalline permanent magnets, grain surfaces in general are not perfect.²¹ Within thin surface layers of about 1–2 nm,²⁴ inhomogeneities of the material parameters like exchange constant, anisotropy constant, or spontaneous magnetic polarization are expected. Figure 8 shows the structure for two different grain diameters with intergranular layers used for numerical calculations. (See Fig. 9 also.) Neighboring grains are separated by a layer with a constant thickness

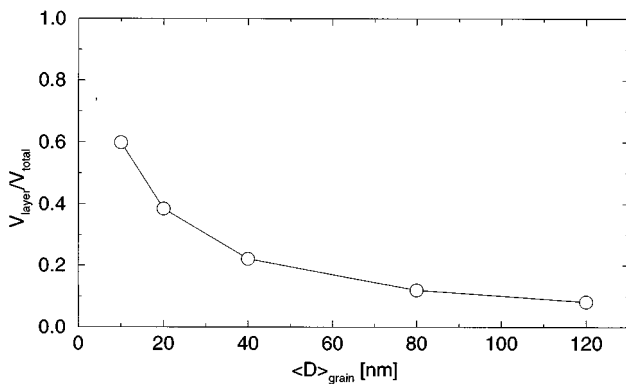


FIG. 9. Volume fraction of intergranular layers $V_{\text{layer}}/V_{\text{total}}$ for different mean grain diameters of the structure presented in Fig. 8. The volume fraction of intergranular layers decreases from 60% at $\langle D \rangle_{\text{grain}} \approx 10 \text{ nm}$ to 8% at $\langle D \rangle_{\text{grain}} \approx 120 \text{ nm}$.

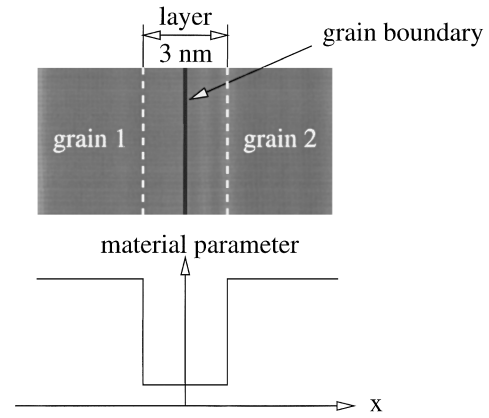


FIG. 10. Situation near grain boundaries: Selected material parameters (A , K_1 , K_2 , and/or J_s) are reduced within 1.5 nm surround each grain (or 3 nm between adjacent grains).

of exactly 3 nm. Within these layers, selected material parameters are reduced by a constant factor with respect to the bulk values (see schematic, Fig. 10). The easy-axis direction near the grain surface is the same as in the bulk. Such a grain structure allows one to investigate systematically the influence of reduced material parameters near grain boundaries on demagnetization processes in nanoscaled permanent magnets.

A. Effect of exchange-coupling between adjacent grains

As a result of Sec. III B 2, the exchange coupling between adjacent grains is responsible for the enhancement of the remanence as well as the reduction of the coercive field in nanoscaled isotropic magnets. With increasing grain diameter these effects become less significant, because of the limited range of exchange interactions ($\delta_B \approx 4.2 \text{ nm}$ for $\text{Nd}_2\text{Fe}_{14}\text{B}$). Therefore, we expect with reduced exchange constant between adjacent grains a decrease of the remanence and an increase of the coercive field especially for grains smaller than 20 nm. This is confirmed by the results shown in Fig. 11, where the remanence and the coercive field as a function of the mean grain diameter for three different types of intergranular layers are represented: (a) ideally coupled grains (no layers), (b) only reduction of the exchange constant to 10% of the bulk values ($A = 7.7 \times 10^{-13} \text{ J/m}$), and (c) only reduction of the exchange constant to 1% of the bulk values ($A = 7.7 \times 10^{-14} \text{ J/m}$). All other material parameters remain constant. The reduction of the exchange constant to 10% of the bulk values is sufficient to obtain significant changes in the magnetic properties: the remanence decreases by about 5% for $\langle D \rangle_{\text{grain}} = 10 \text{ nm}$ (2.5% for $\langle D \rangle_{\text{grain}} = 120 \text{ nm}$) and the coercive field becomes grain size independent. The typical logarithmic decrease of the remanence is preserved, whereas the increase of the coercive field up to 50 nm vanishes completely. According to Fig. 11, a further reduction of the exchange constant to 1% of the bulk values within the layers causes no further remarkable changes in both magnetic properties. So we can conclude that already a small reduction of the intergrain exchange interaction significantly affects the remanence and coercive field in the above described way.

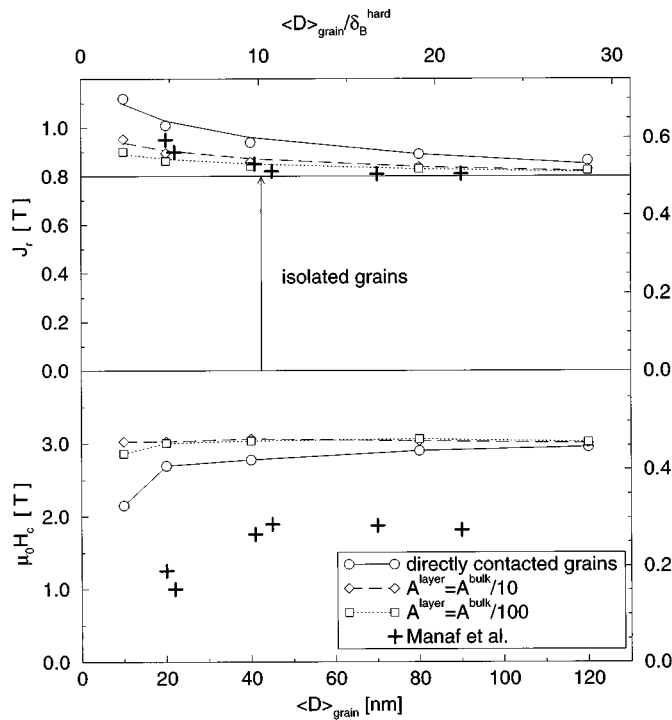


FIG. 11. Remanence and coercive field as a function of the mean grain diameter for the isotropic $\text{Nd}_2\text{Fe}_{14}\text{B}$ magnet with reduced exchange constant between adjacent grains.

B. Effect of magnetocrystalline anisotropy between adjacent grains

The magnetocrystalline anisotropy is responsible for the magnetic hardness of permanent magnets. The greater the anisotropy constant of the magnetic material, the greater the coercive field. Now we locally reduce the magnetocrystalline anisotropy near grain boundaries within layers of about 3 nm. According to Fig. 9, the volume fraction of intergranular layers on the total volume decreases from 60% for $\langle D \rangle_{\text{grain}} \approx 10$ nm to 8% for $\langle D \rangle_{\text{grain}} \approx 120$ nm. Within this volume fraction, the permanent magnet is magnetically softened. Figure 12 shows the results for the remanence and coercive field as a function of the mean grain diameter for following three types of intergranular layers: (a) directly contacted grains (as reference), (b) only reduction of the anisotropy constant to 10% of the bulk values ($K_1 = 4.30 \times 10^5 \text{ J/m}^3$, $K_2 = 0.65 \times 10^5 \text{ J/m}^3$), and (c) only reduction of the anisotropy constant to 1% of the bulk values ($K_1 = 4.30 \times 10^4 \text{ J/m}^3$, $K_2 = 0.65 \times 10^4 \text{ J/m}^3$). All other material parameters within the layers coincide with the bulk values. Similar to the previous section, a significant change of magnetic properties just exists by decreasing the anisotropy constant between adjacent grains to 10% of the bulk values: the remanence increases between 3 and 16% and the coercive field decreases between 20 and 50% (see Fig. 12). But the qualitative behavior of the remanence as well as of the coercive field with increasing mean grain diameter is the same as for directly contacted grains. This is easy to understand. Within the intergranular layers with reduced anisotropy constant, the magnetization distribution is mainly determined by exchange interactions and not by the easy axes. So the intergrain exchange interactions become more effective, which leads to a

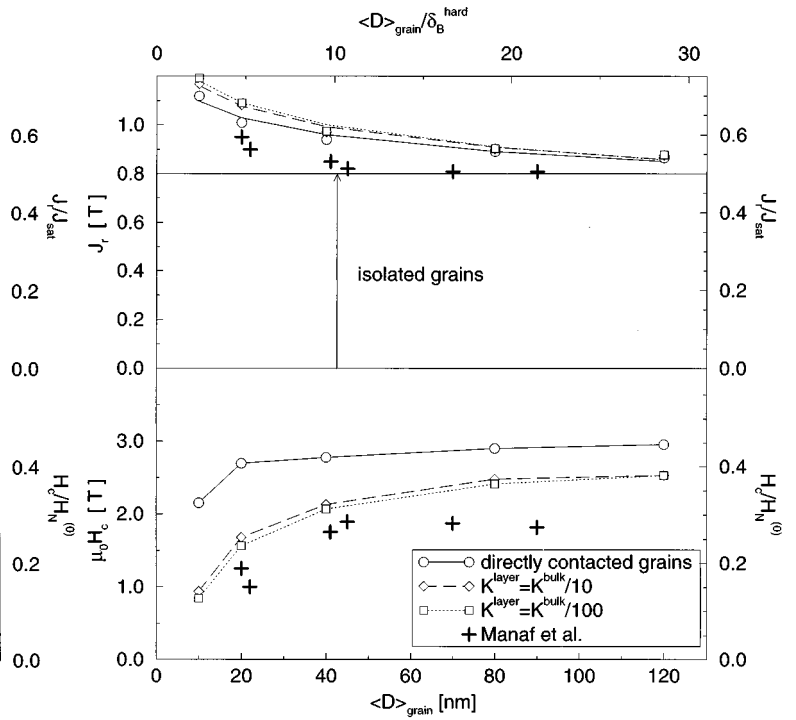


FIG. 12. Remanence and coercive field as a function of the mean grain diameter for the isotropic $\text{Nd}_2\text{Fe}_{14}\text{B}$ magnet with reduced magnetocrystalline anisotropy between adjacent grains.

further enhancement of the remanence and a loss of the coercive field (see Sec. III B 2). But the strong decline of the coercive field by nearly a factor of 2 cannot be completely attributed to the more effective intergrain exchange interactions due to reduced magnetocrystalline anisotropy between adjacent grains. For a mean grain diameter of about 10 nm, the volume fraction of intergranular phases is yet 60%. A reduction of the magnetocrystalline anisotropy within this great part of the magnet is equal to a magnetic softening of the material. Since the volume fraction of intergranular layers decreases with increasing grain size (see Fig. 9), the coercive field increases.

C. Effect of spontaneous magnetic polarization near grain boundaries

The development of new magnetic materials tries to enhance the spontaneous magnetic polarization and to preserve a high magnetocrystalline anisotropy. The greater the spontaneous magnetic polarization, the greater the chance to achieve a high remanence. But in the presence of regions with reduced spontaneous magnetic polarization between adjacent grains, the resulting average magnetization of the whole magnet and so the remanence decreases. Figure 13 shows the grain size dependence of the remanence and of the coercive field for three different types of intergranular phases: (a) without any layers, (b) only reduced spontaneous magnetic polarization to 10% of the bulk ($J_s = 0.16 \text{ T}$), and (c) only reduced spontaneous magnetic polarization to 1% of the bulk ($J_s = 0.016 \text{ T}$). The other material parameters are identical with the bulk values.

In contrast to ideally coupled grains, the remanence increases with increasing mean grain diameter in the presence

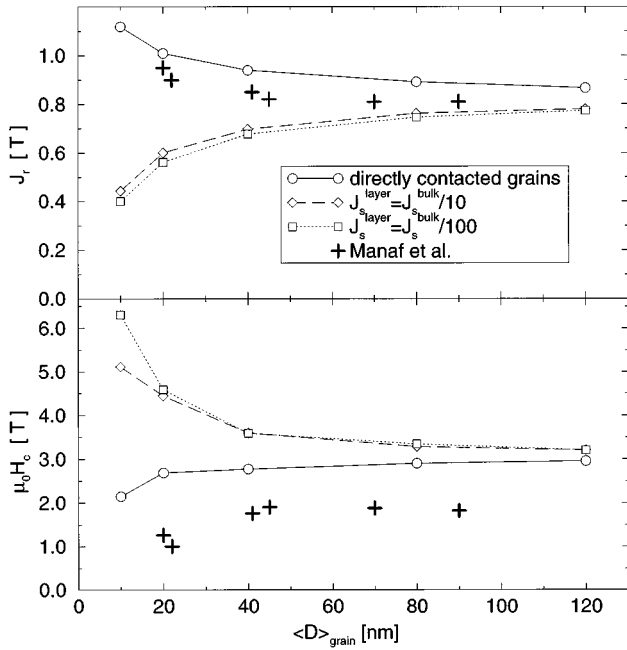


FIG. 13. Remanence and coercive field as a function of the mean grain diameter for the isotropic $\text{Nd}_2\text{Fe}_{14}\text{B}$ magnet with reduced spontaneous magnetic polarization between adjacent grains.

of intergranular layers (see Fig. 13). With decreasing volume fraction of the intergranular layers (see Fig. 9), the resulting average magnetization in the z direction and therefore the remanence becomes greater. According to Fig. 14, the normalized remanence J_r/J_{sat} shows a logarithmic decrease with increasing grain diameter similar to ideally coupled grains. So the increase of the remanence with the grain size can be entirely attributed to the reduced values of J_s near grain

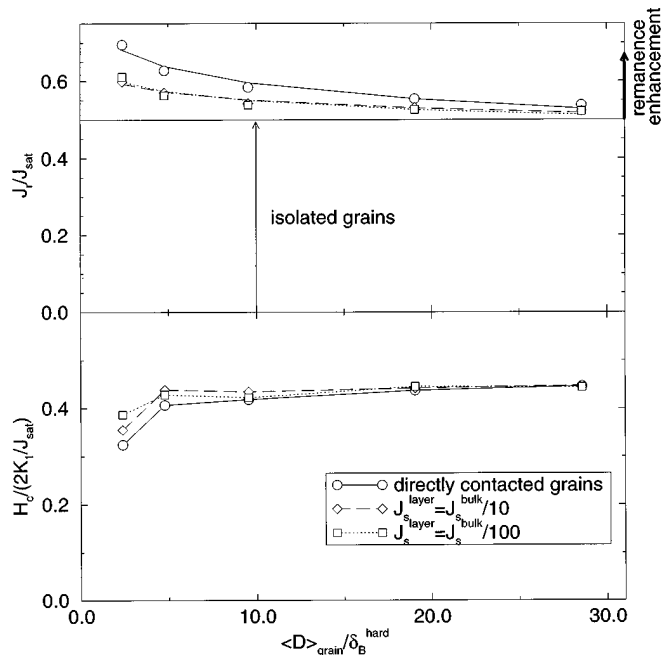


FIG. 14. The same as in Fig. 13. But now for the normalized remanence and coercive field.

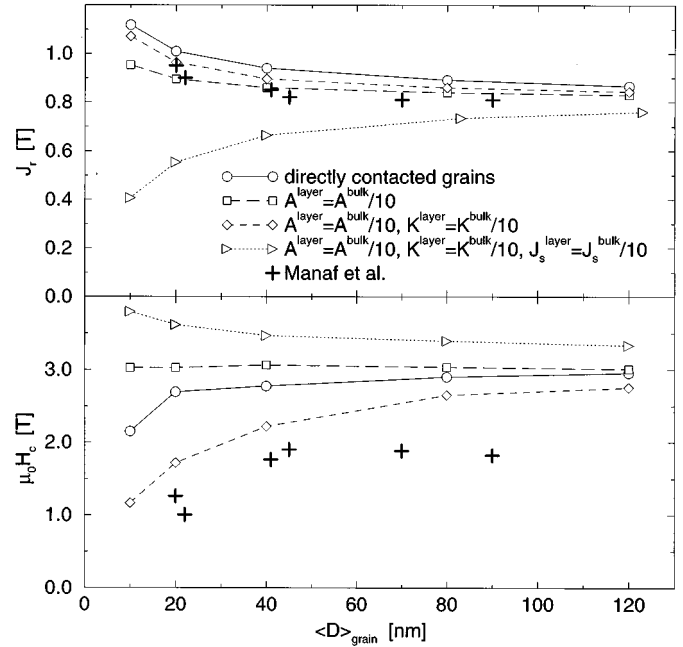


FIG. 15. Reduction of more than one material parameter near grain boundaries for the isotropic $\text{Nd}_2\text{Fe}_{14}\text{B}$ magnet presented in Fig. 8.

boundaries. For all grain sizes, the remanence enhancement due to exchange interactions is less effective than the reduction due to the diminished average magnetization (compare Figs. 13 and 14).

For ideally coupled grains, the coercive field increases for a mean grain diameter smaller than 50 nm. This situation qualitatively changes with reduced J_s between neighboring grains. According to Fig. 13, the coercive field monotonously decreases with increasing mean grain diameter. Obviously, the reduction of J_s near grain boundaries leads to an enhancement of the coercive field, even if all other material parameters (especially K_i) are kept constant. The influence of the decreasing average magnetization with decreasing mean grain size can be eliminated by plotting the normalized coercivity $H_c/(2K_1/J_{\text{sat}})$ as a function of the mean grain diameter $\langle D \rangle_{\text{grain}}$ (see Fig. 14). The so normalized coercive field increases with the grain diameter similar to directly contacted grains. As a result, the effect of decreasing coercive field $\mu_0 H_c$ with increasing grain diameter $\langle D \rangle_{\text{grain}}$ can be entirely attributed to the increase of the net magnetization [compare also Eq. (2)].

D. Combination of all effects

With the background of the previous three sections, we can understand the changes in magnetic properties by reducing simultaneously the exchange constant, anisotropy constant, and spontaneous magnetic polarization between adjacent grains. Since the reduction of the material parameters near grain boundaries to 1% of the bulk values nearly gives the same as for 10%, Fig. 15 only shows the results for the latter case. As described in Sec. IV A, the reduction of the exchange constant leads to a decrease in the remanence and a grain-size independent coercive field (see squares of Fig. 15). Starting from this situation, an additional reduction of the

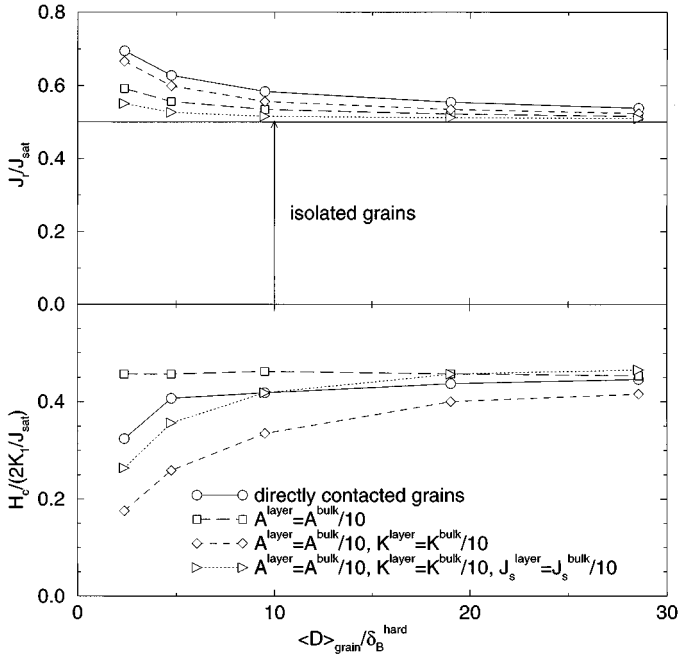


FIG. 16. The same as in Fig. 15. But now for the normalized remanence and coercive field.

magnetocrystalline anisotropy causes an enhancement of the remanence and reduces the coercive field in particular for small grains (see diamonds of Fig. 15). That is exactly the behavior, we expect by Sec. IV B. A further reduction of the spontaneous magnetic polarization qualitatively changes the dependence of the magnetic properties with increasing mean grain diameter (see triangles of Fig. 15): the remanence increases and the coercive field decreases smoothly. Figure 16 shows the same for the normalized remanence and coercivity. This is in agreement with Sec. IV C. As a result, the disturbance of one or more material parameters (like A , K_1 , K_2 , or J_s) near grain boundaries leads to characteristic changes of the remanence and coercive field as a function of the mean grain size of nanoscaled isotropic magnets.

V. COMPARISON WITH EXPERIMENTAL RESULTS

Manaf *et al.*⁵ experimentally investigated the grain-size dependence of magnetic properties like remanence and coercive field for melt-spun NdFeB magnets (exact composition $\text{Nd}_{13.2}\text{Fe}_{79.2}\text{B}_6\text{Si}_{1.2}$). Their results are drawn in Figs. 11, 12, 13, and 15 by strong plus signs. In the case of ideally coupled grains, the computed and experimentally obtained grain size dependences of the remanence and of the coercive field are almost identical. Differences only exist in absolute values: the computed remanence is of about 0.1 T and the coercive field of about 1.0 T greater than the corresponding experimental values.

According to Fig. 11, the computed remanence gets across the experimental values by reducing the exchange constant between adjacent grains. But to achieve a coercive field closer to experimental values, a reduction of the magnetocrystalline anisotropy near grain boundaries as shown in Fig. 12 is necessary. According to Fig. 15, the best possible coincidence with experiment is given by using a model mag-

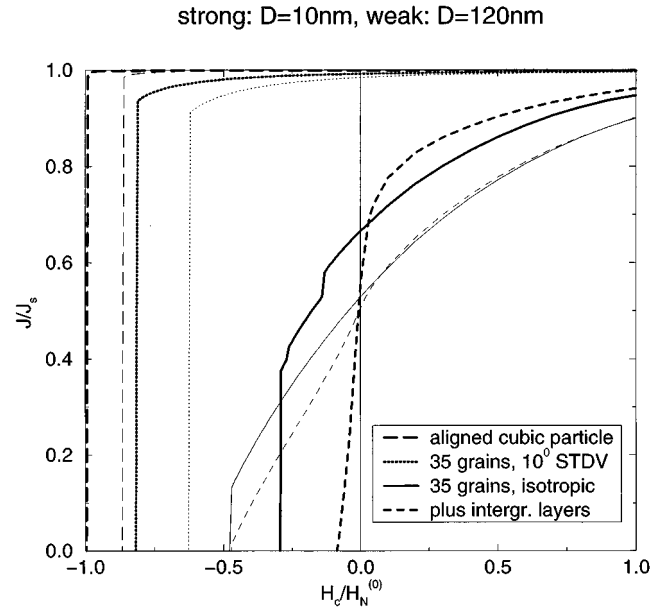


FIG. 17. Remanence as a function of the applied field for different grain arrangements (aligned cubic particle, 35 grains with Gaussian distribution of easy axis, 35 grains with isotropic distribution of easy axis and reduced material parameters near grain boundaries: $A^{\text{layers}}=A^{\text{bulk}}/100$, $K_i^{\text{layers}}=K_i^{\text{bulk}}/100$). The steps in the demagnetization curves vanish with increasing complexity of the grain structure. J_s is the spontaneous polarization and $H_N^{(0)}=2K_1/J_s$ the ideal nucleation field.

net with reduced exchange constant and magnetocrystalline anisotropy within thin surface layers of about 1.5 nm surround each grain.

VI. SHAPE OF DEMAGNETIZATION CURVES AND MAXIMUM ENERGY PRODUCT

The shape of demagnetization curves sensitively depends on microstructural properties. Figure 17 shows typical demagnetization curves for simple and more complex grain arrangements.

As expected, the demagnetization curve of the perfectly aligned cubic particle is almost rectangular (see long-dashed curves of Fig. 17). For an edge length of 10 nm, the resulting magnetization in the z direction keeps constant until the ideal nucleation field $H_N^{(0)}=2K_1/J_s$ is reached. After that all magnetic moments spontaneously reverse their directions, which leads to a strong step in the demagnetization curve. With increasing edge length, the larger strayfields cause only a reduction of the coercive field but the shape of the demagnetization curve remains constant (compare strong and weak long-dashed curves of Fig. 17).

A more complicated case represents an ensemble of 35 directly contacted grains with different distributions of easy axes. For such magnets, the demagnetization process looks similar to a cubic particle: As a result of intergrain interactions, the demagnetization curves are generally characterized by sections with nearly vertical steps (see dotted and solid

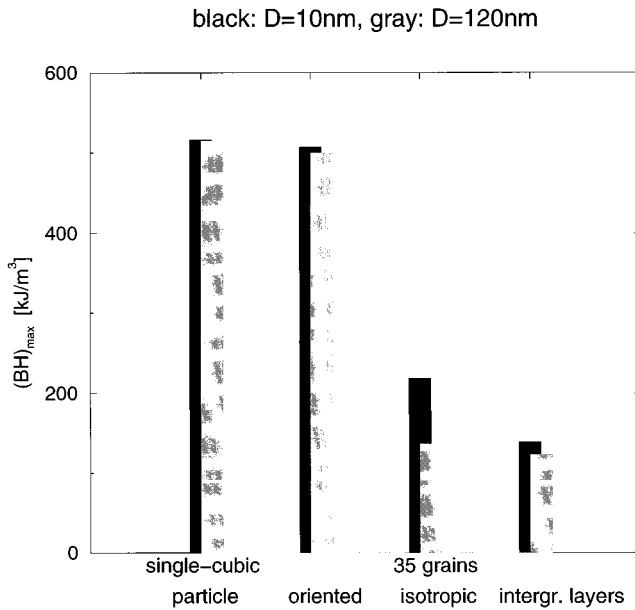


FIG. 18. Dependence of the maximum energy product on the microstructure and the mean grain diameter obtained by the demagnetization curves of Fig. 17.

curves of Fig. 17). But with increasing misorientation of the magnetic particles, the resulting magnetization in the z direction decreases by rotations more and more with the applied field and consequently the steps become smaller (compare dotted with solid curves of Fig. 17). Such steps may be determined by the nucleation fields of individual particles. Only one step exists, if the magnetization reversal of one particle is sufficient to reverse also the magnetic environment.

For ensembles of grains with reduced intergrain interactions, all steps in the demagnetization curves vanish (see dashed lines in Fig. 17). The resulting magnetization in the z direction monotonously decreases with the applied field. The magnetization reversal of each particle nearly proceeds independently from the others. Because short-range exchange interactions are suppressed, only long-range dipolar interactions influence neighboring grains. But in nanoscaled dimensions strayfield effects play only a minor role (see Sec. III A 2). Figure 18 shows the maximum energy products calculated as described in Sec. II A 3 for the above-mentioned grain arrangements. With a high remanence, a high coercive field, and nearly perfect rectangular demagnetization curve, the single cubic particle possesses a maximum energy product of about 515 kJ/m^3 . With increasing edge length of the cube the coercive field decreases. But the maximum energy product nearly remains constant. This holds also for the ensemble of 35 grains with a Gaussian distribution of easy axes of about 10° with respect to the aligned field. A significant decrease of the maximum energy product exists by going to isotropically distributed grains (see Fig. 18). This can be attributed to the following effects: (a) the decreasing remanence, (b) the decreasing coercive field, and (c) the loss of rectangularity of the demagnetization curves (see Fig. 17). The same effect exists in the presence of intergranular layers.

VII. SUMMARY

The magnetic properties of a single sphere are mainly determined by the intrinsic material parameters and the angle between the easy axis and the applied field (“misorientation”). If the misorientation reaches 90° , both the remanence and the coercive field gets across zero (see Fig. 2). For small nonspherical grains of about 10 nm, local strayfields are neglectable and do not affect the demagnetization process. But with increasing grain size, the magnetization distribution gets more nonuniform, which can be clearly attributed to long-range dipolar interactions. Even at $\langle D \rangle_{\text{grain}} = 120 \text{ nm}$, the local strayfields cause no remarkable changes in the remanence. Only the coercive field is reduced by 16% of $H_N^{(0)}$ for a cubic grain. So we can conclude, that strayfields play a minor role in nanoscaled dimensions. An ensemble of perfectly aligned grains without any intergranular phases exactly behaves like a single particle with the same extension. Differences only appear in the presence of misorientations of easy axes or intergranular phases. Even for a Gaussian distribution of easy axes with a standard deviation of 10° , the remanence and coercive field qualitatively show the same grain size dependence as the cubic particle (see Fig. 3). Similar to a single cube, misoriented grains and local strayfields mainly control the magnetization reversal. For an isotropic distribution of easy axes intergrain exchange interactions additionally become important. These interactions are responsible for an enhancement of remanence with respect to non-interacting particles and a further reduction of coercive field. Because of the short-range character of exchange interactions ($\delta_B \approx 4.2 \text{ nm}$ for $\text{Nd}_2\text{Fe}_{14}\text{B}$), these effects become smaller with increasing grain size: the remanence decreases and the coercive field increases (see Fig. 3).

The best possible coincidence between numerical and experimental investigations can be achieved by reducing the exchange constant and magnetocrystalline anisotropy near grain boundaries. A reduction of intergrain exchange interactions cause a decrease of the remanence and an increase of the coercive field especially for small grains of about 10 nm. An additional reduction of the magnetocrystalline anisotropy is identical with magnetic softening and leads so to a decrease of the coercive field. If the material parameters are disturbed within a region of 3 nm between adjacent grains, their reduction to 10% of the bulk values nearly gives the same results for experiment and theory (see Fig. 15).

The numerical calculations show that an enhancement of the remanence in isotropic nanoscaled permanent magnets is always accompanied by a reduction of the coercive field and vice versa. For ideally coupled grains or reduced A or K_i between adjacent grains (see Figs. 11 and 12), the remanence decreases and the coercive field increases with the mean grain diameter. With reduced J_s near grain junctions (see Fig. 13), the opposite behavior can be observed.

With increasing complexity of the grain structure, the shape of demagnetization curves changes characteristically. In the presence of intergranular layers with reduced material parameters, the demagnetization curves possess no steps and the magnetization reversal continuously proceeds with the applied field. Steps are typical for the demagnetization process of ideal Stoner-Wohlfarth particles and are in general not observed by experiment.

- ¹R. W. McCallum, A. M. Kadin, G. B. Clemente, and J. E. Keem, *J. Appl. Phys.* **61**, 3577 (1987).
- ²M. Sagawa, S. Hirose, H. Yamamoto, S. Fujimura, and Y. Matsuura, *Jpn. J. Appl. Phys.* **26**, 785 (1987).
- ³L. Schultz, J. Wecker, and E. Hellstern, *J. Appl. Phys.* **61**, 3583 (1987).
- ⁴G. B. Clemente, J. E. Keem, and J. P. Bradley, *J. Appl. Phys.* **64**, 5299 (1988).
- ⁵A. Manaf, R. A. Buckley, H. A. Davies, and M. Leonowicz, *J. Magn. Magn. Mater.* **101**, 360 (1991).
- ⁶L. Schultz, *Mater. Sci. For.* **88-90**, 687 (1992).
- ⁷P. McCormick, J. Ding, Y. Liu, and R. Street, in *Proceedings of the 2nd International Conference on Structural Applications of Mechanical Alloying*, edited by J. de Barbadillo, H. Fores, and R. Schwarz (ASM, Materials Park, OH, 1993), pp. 349–352.
- ⁸J. Ding, P. G. McCormick, and R. Street, *J. Magn. Magn. Mater.* **124**, 1 (1993).
- ⁹J. Ding, P. McCormick, and R. Street, in *8th International Symposium on Magnetic Anisotropy and Coercivity in Rare Earth-Transition Metal Alloys*, Birmingham, 1994, edited by C. Manwaring, D. Jones, A. Williams, and I. Harris (The University of Birmingham, Edgbaston, 1994), pp. 63–70.
- ¹⁰J. Ding, P. McCormick, and R. Street, *J. Magn. Magn. Mater.* **135**, 200 (1994).
- ¹¹H. Davies, in *8th International Symposium on Magnetic Anisotropy and Coercivity in Rare Earth-Transition Metal Alloys* (Ref. 9), pp. 456–473.
- ¹²J. Croat, in *8th International Symposium on Magnetic Anisotropy and Coercivity in Rare Earth-Transition Metal Alloys* (Ref. 9), pp. 65–78.
- ¹³J. M. D. Coey, *J. Magn. Magn. Mater.* **140-144**, 1041 (1995).
- ¹⁴O. Yoshichika, L. Hong-shuo, and J. M. D. Coey, *IEEE Trans. Magn.* **26**, 2658 (1990).
- ¹⁵T. Schrefl, H. F. Schmidts, J. Fidler, and H. Kronmüller, *J. Magn. Magn. Mater.* **124**, 251 (1993).
- ¹⁶T. Schrefl, H. F. Schmidts, J. Fidler, and H. Kronmüller, *J. Appl. Phys.* **73**, 6510 (1993).
- ¹⁷T. Schrefl, H. F. Schmidts, J. Fidler, and H. Kronmüller, *IEEE Trans. Magn.* **29**, 2878 (1993).
- ¹⁸H. Kronmüller, T. Schrefl, R. Fischer, and J. Fidler, in *8th International Symposium on Magnetic Anisotropy and Coercivity in Rare Earth-Transition Metal Alloys* (Ref. 9) pp. 1–24.
- ¹⁹R. Fischer, T. Schrefl, H. Kronmüller, and J. Fidler, *J. Magn. Magn. Mater.* **153**, 35 (1996).
- ²⁰A. Manaf, P. Zhang, I. Ahmed, H. Davies, and R. Buckley, *IEEE Trans. Magn.* **29**, 2866 (1993).
- ²¹M. T. Clavaguera-Mora, J. A. Diego, N. Clavaguera, A. Hernandez, and M. Vázquez, *J. Appl. Phys.* **76**, 1124 (1994).
- ²²J. Liu, I. Ahmad, A. Davies, P. Zhang, S. Huo, and R. Buckley, in *8th International Symposium on Magnetic Anisotropy and Coercivity in Rare Earth-Transition Metal Alloys* (Ref. 9), pp. 161–167.
- ²³I. Ahmad, M. Al-Khafaji, A. Davies, R. Buckley, and W. Rainforth, in *8th International Symposium on Magnetic Anisotropy and Coercivity in Rare Earth-Transition Metal Alloys* (Ref. 9), pp. 145–152.
- ²⁴A. Zern, Master's thesis, Universität Stuttgart, Deutschland, 1995.
- ²⁵E. C. Stoner and E. P. Wohlfarth, *Philos. Trans. R. Soc. London Ser. A* **240**, 599 (1948).
- ²⁶G. C. Hadjipanayis and W. Gong, *J. Appl. Phys.* **64**, 5559 (1988).
- ²⁷W. F. Brown, Jr., *Rev. Mod. Phys.* **17**, 15 (1945).
- ²⁸H. Kronmüller, *Phys. Status Solidi B* **144**, 385 (1987).
- ²⁹R. Fischer, T. Schrefl, H. Kronmüller, and J. Fidler, *J. Magn. Magn. Mater.* **150**, 329 (1995).
- ³⁰H. Zijlstra, in *Ferromagnetic Materials*, edited by E. P. Wohlfarth (North-Holland Physics, Amsterdam, 1982).
- ³¹E. F. Kneller and R. Hawig, *IEEE Trans. Magn.* **27**, 3588 (1991).
- ³²H. Kronmüller, K. D. Durst, S. Hock, and G. Martinek, *J. Phys. (Paris) Colloq.* **49**, CC8-623 (1988).
- ³³S. Hock, Ph.D. thesis, Universität Stuttgart, Deutschland, 1988.
- ³⁴T. Schrefl, J. Fidler, and H. Kronmüller, *J. Magn. Magn. Mater.* **138**, (1994).
- ³⁵P. E. Gill, W. Murray, and M. H. Wright, *Practical Optimization* (Academic, London, 1981).
- ³⁶R. H. Victora, *Phys. Rev. Lett.* **58**, 1788 (1987).
- ³⁷M. E. Schabes, *J. Magn. Magn. Mater.* **95**, 249 (1991).
- ³⁸J. G. Zhu and H. N. Bertram, *J. Appl. Phys.* **63**, 3248 (1988).
- ³⁹R. H. Victora, C. F. Brucker, and F. E. Spada, *J. Magn. Magn. Mater.* **97**, 343 (1991).
- ⁴⁰R. C. Giles and M. Mansuripur, *J. Magn. Soc. Jpn.* **17**, 255 (1993).
- ⁴¹Y. Nakatani, Y. Uesaka, and N. Hayashi, *Jpn. J. Appl. Phys.* **28**, 2485 (1989).
- ⁴²M. Mansuripur, *J. Appl. Phys.* **63**, 5809 (1988).
- ⁴³W. Chen, D. R. Fredkin, and T. R. Koehler, *IEEE Trans. Magn.* **29**, 2124 (1993).
- ⁴⁴D. Berkov, K. Ramstöck, and A. Hubert, *Phys. Status Solidi A* **137**, 207 (1993).
- ⁴⁵J. C. Mallinson, *IEEE Trans. Magn.* **23**, 2003 (1987).
- ⁴⁶W. F. Brown, Jr., *IEEE Trans. Magn.* **15**, 1196 (1979).
- ⁴⁷A. Lyberatos and R. Chantrell, *IEEE Trans. Magn.* **26**, 2119 (1990).
- ⁴⁸G. Martinek and H. Kronmüller, *J. Magn. Magn. Mater.* **86**, 177 (1990).
- ⁴⁹H. F. Schmidts and H. Kronmüller, *J. Magn. Magn. Mater.* **129**, 329 (1994).
- ⁵⁰H. F. Schmidts and H. Kronmüller, *J. Magn. Magn. Mater.* **129**, 361 (1994).
- ⁵¹M. E. Schabes and H. N. Bertram, *J. Appl. Phys.* **64**, 1347 (1988).
- ⁵²Y. Uesaka, Y. Nakatani, and N. Hayashi, *J. Magn. Magn. Mater.* **145**, 205 (1995).